J. Fluid Mech. (1996), *vol.* 324, *pp.* 181–198

Taylor–Couette instability of travelling waves with a continuous spectrum

By S. GHOSH MOULIC† AND L. S. YAO
Department of Mechanical and Aerospace Engineering, Arizona State University, Tempe, AZ 85287-6106, USA

(Received 12 May 1994 and in revised form 19 April 1996)

The nonlinear evolution of a continuous spectrum of travelling waves resulting from the growth of unstable disturbances in circular Couette flow has been investigated. Numerical solution of the governing integro-differential equations for different initial conditions shows that the equilibrium states of Taylor-vortex, wavy-vortex or spiral-vortex flows are not unique, but depend on the initial disturbance. The presence of multiple solutions at a fixed Reynolds number for a given Taylor–Couette geometry has been known since Coles' seminal contribution in 1965. The current study indicates that the equilibrium state of flows on a stable bifurcation branch is a natural consequence of nonlinear wave resonance and is dependent on the initial conditions. The resulting wavenumber can take any value within an accessible finite band. Since such multiple solutions have also been found numerically for mixed-convection flows and experimentally for several other flows, there is evidence to support the conclusion that a non-uniqueness in the sense of Coles is a generic property for all fluid flows.

1. Introduction

The study of the stability and transitions of flow between concentric rotating cylinders is a topic of fundamental importance in fluid dynamics. Taylor (1923) demonstrated theoretically and experimentally that circular Couette flow becomes unstable when the speed of the inner cylinder is increased beyond a certain critical value. His experiments showed that the instability leads to a new steady axisymmetric secondary flow in the form of regularly spaced vortices in the axial direction. Coles (1965) observed that this axisymmetric Taylor-vortex flow becomes unstable as the angular speed of the inner cylinder is increased further, beyond a second critical value. This instability results in a wavy-vortex flow, with azimuthally propagating waves superposed on the Taylor vortices. Coles found that the spatial structure of the wavy-vortex flow, characterized by axial and aximuthal wavenumbers, is not a unique function of the Reynolds number and boundary conditions. Different equilibrium states could be achieved at the same Reynolds number by approaching the final Reynolds number with different acceleration rates, and by rotating and then stopping the outer cylinder. Fenstermacher, Swinney & Gollub (1979) studied the transition to turbulence in Taylor–Couette flow using a laser-Doppler anemometer. They also found that the different spatial states had different spectra and transition Reynolds numbers. Presumably, these different final states at the same value of the Reynolds number are functions of the initial conditions. The multiple equilibrium states in Taylor–Couette

† Present address, Department of Mechanical Engineering, Indian Institute of Technology, Bombay, India.

flow are studied in this investigation by means of a formulation which considers nonlinear interactions among waves of all possible wavenumbers.

The non-uniqueness of the equilibrium state observed by Coles (1965) was subsequently observed in time-independent Taylor-vortex flow by Snyder (1969), Burkhalter & Koschmieder (1974) and Benjamin (1978). Snyder (1969) found that, while the wavelength at the onset of instability was unique, Taylor-vortex flows with different wavenumbers could be obtained at the same value of the Reynolds number by varying the initial conditions. He observed that there was a band of accessible wavenumbers, smaller than the band that can grow according to linear theory. This is known as a sideband instability. Burkhalter & Koschmieder (1974) found that the range of axial wavelengths for stable Taylor-vortex flow is quite large. Benjamin (1978) observed different spatial states even in an annulus so short that only three or four vortices could be accommodated. The nonlinear interactions among Taylor vortices with different wavenumbers were studied by Yao & Ghosh Moulic (1995*a*) using a weakly nonlinear theory formulated with a continuous spectrum. They represented the disturbance by a Fourier integral and derived an integro-differential equation for the evolution of the amplitude density function of a continuous spectrum. Numerical solution of this integro-differential equation indicated that the equilibrium state of the flow depends on the wavenumber and amplitude of the initial disturbance, as observed experimentally. Their results also show that sideband instability is a consequence of nonlinear resonance among interacting waves. Yao & Ghosh Moulic (1995*a*) show that *the quadratic inertia terms in the Navier–Stokes equations can be interpreted as nonlinear wave resonances of triads, quartets, and so forth.* They further showed that nonlinear wave resonance is the fundamental mechanism responsible for the occurrence of side-band instability, secondary instability, flow bifurcation, and turbulent energy cascade.

The linear stability of circular Couette flow to non-axisymmetric disturbances has been studied by DiPrima (1961) and by Krueger, Gross & DiPrima (1966). Using the small-gap approximation, they found that, when the outer cylinder is at rest, the critical Taylor number for non-axisymmetric disturbances was higher than the critical Taylor number for axisymmetric disturbances. The instability of Taylor-vortex flow to wavy-vortex disturbances has been studied by Davey, DiPrima & Stuart (1968) using the small-gap approximation. They considered the weakly nonlinear interactions between two axisymmetric Taylor-vortex modes and two non-axisymmetric instability modes of circular Couette flow. They found that the Taylor-vortex flow becomes unstable at a critical Taylor number which is about 8% above the critical value at which Taylor vortices first appear. They also showed that, after instability, a new equilibrium flow with wavy boundaries between cells is established. Marcus (1984) solved the time-dependent Navier–Stokes equations numerically using a spectral method to simulate Taylor–Couette flow. He computed several stable axisymmetric Taylor-vortex flows and several stable non-axisymmetric wavy-vortex flows that correspond to one travelling wave. His results suggest that the travelling waves arise from a secondary instability caused by the strong radial motion in the outflow boundaries of the Taylor vortices.

In this investigation, we study the nonlinear stability of circular Couette flow to non-axisymmetric disturbances. The disturbance is represented in its most general form by a Fourier integral over all possible axial wavenumbers and a Fourier series over the integer azimuthal wavenumbers. This allows energy transfer among all possible interacting waves; consequently, it can predict the evolution of a disturbance from an arbitrary initial waveform. The Fourier components of the disturbance quantities are

expanded in a series of the linear-stability eigenfunctions. The eigenfunction expansion reduces the Navier–Stokes equations to a system of nonlinearly coupled integro-differential equations for the amplitude-density functions of a continuous spectrum (Yao & Ghosh Moulic 1995*b*).

The integro-differential equations have been solved numerically with different initial conditions. The infinite range of integration is truncated to a finite range, and the integrals are discretized using the trapezoidal rule. The numerical approximations effectively reduce the Fourier integrals to Fourier series; consequently, the numerical solutions show a periodicity in the axial direction. It is important to have the computational domain large enough to include all instability waves and their harmonics in order to realistically simulate the physics of the problem.

The results have been checked with the direct numerical simulation of the time-dependent Navier–Stokes equations using a Fourier–Chebyshev spectral method. It is worth noting that the numerical solution of the integro-differential equations is computationally more efficien than a Fourier–Chebyshev spectral method (Yao & Ghosh Moulic 1994). The method of eigenfunction expansion employed in the present investigation uses the same scalar amplitude-density function for each mode for the velocity components and pressure. Thus, the three momentum equations and the continuity equation are reduced to a single set of equations for the amplitude-density functions. This results in a substantial reduction of the computational effort. The eigenfunction expansion eliminates one of the major difficulties associated with the direct numerical simulation of the incompressible Navier–Stokes equations, namely the requirement of a simultaneous enforcement of the no-slip boundary condition and the incompressibility constraint. Kleiser & Schumann (1980) devised an influence-matrix method to accommodate these requirements. Their algorithm requires the solution of six Helmholtz equations at each time step. In the current investigation, the eigenfunctions used in the expansion are solutions of the linearized Navier–Stokes equations; hence, they individually satisfy the incompressibility constraint and the no-slip boundary conditions. This results in a considerable simplification of the numerical procedure. Therefore, the CPU time required for the numerical solution of the set of governing integro-differential equations is only *one-sixth* of the CPU time required for the direct numerical simulation using a Fourier–Chebyshev spectral method. The current formulation provides a new efficient algorithm for the solution of the Navier–Stokes equations, and can be used for the direct simulation of turbulent flows which are homogeneous in two directions. The extension of the formulation to problems without this limitation is straightforward.

Results have been obtained for rotationally symmetric Taylor-vortex flow at $Re = 88.1$ and $\eta = 0.5$ and non-rotationally symmetric wavy-vortex or spiral-vortex flows at $Re = 162$ and $\eta = 0.874$, where η is the ratio of the radii of the inner and outer cylinders, and Re is the Reynolds number. The results indicate that the equilibrium state of Taylor-vortex, wavy-vortex and spiral-vortex flows depends on the initial conditions, as observed experimentally, and is not unique. Multiple equilibrium states with different wavenumbers are found to exist at fixed values of η and the Reynolds number. These equilibrium states are stable to perturbations of small amplitudes and are physically realizable. We have also found that the stable equilibrium state can be shifted to a new stable equilibrium state by a finite-amplitude disturbance. The results suggest that the selection of the equilibrium wavenumber is a natural consequence of nonlinear wave resonance which depends on the initial conditions. The existence of multiple stable equilibrium states implies that the torque induced by the fluid motion cannot be uniquely determined. Since an initial condition, or an ambient disturbance

in a real engineering system, cannot usually be determined owing to the presence of background noise, an uncertainty associated with non-uniqueness of the flow and lack of knowledge of the initial conditions which influence the equilibrium state of the flow should be taken into account when using any accurately measured values of the torque in engineering design and practice.

The solution of the integro-differential equations for rotationally symmetric Taylor-vortex flow has revealed a new feature. The results indicate that the Taylor-vortex flow is not a purely stationary wave, but consists of standing waves with amplitudes which are much smaller than the amplitude of the dominant stationary vortex for Reynolds numbers in the range of Taylor-vortex flows. Any disturbance which destroys the symmetry of the standing waves can lead to *spiral* flows.

Spiral-vortex flows are found experimentally with a rotating outer cylinder at a much higher Reynolds number than was used in our computations. They seem to be excited by the end conditions of a long annulus. Our model assumes an infinite-long annulus and cannot model the end effects. Our results with the initial condition of single travelling waves along the axial direction show that spiral-vortex flows are possible equilibrium states with a stationary outer cylinder at lower Reynolds number than the experimental value. The phenomenon seems to indicate that the number of possible equilibrium states is enormous, if we know how to excite them.

We would like to emphasize that our computational domain in physical space is several times longer than the wavelengths of all the instability waves. This allows us to study nonlinear interaction among a large number of wave components. This is why we found multiple solutions in our computation. The equilibrium amplitudes of most wave components is very small. However, these wave components participate in nonlinear wave resonance, thereby influencing the final equilibrium state. Our computational model is almost comparable to those used for direct numerical simulations of turbulence for low Reynolds number flows and so is the required CPU time. The average CPU time on a CRAY C90 for our computation is about thirty minutes per case, and the required CPU time to obtain all eigenfunctions of the associated linear stability problem is less than a minute.

2. Analysis

We consider the flow between two concentric cylinders with radii r_1 and r_2, respectively. The inner cylinder rotates with an angular speed Ω, while the outer cylinder is at rest (figure 1). The equations describing the flow are the continuity and Navier–Stokes equations. These equations may be written in dimensionless form as

$$\left.\begin{aligned} \nabla\cdot\boldsymbol{u} &= 0, \\ \frac{\partial \boldsymbol{u}}{\partial t}+\boldsymbol{u}\cdot\nabla\boldsymbol{u} &= -\nabla p+\frac{1}{Re}\nabla^2\boldsymbol{u}, \end{aligned}\right\} \tag{1}$$

where $\boldsymbol{u}=(u,v,w)$, the velocity components in the radial, azimuthal and axial directions respectively, p is the pressure, and t is the time. All lengths have been scaled by the distance between the cylinders, $d=r_2-r_1$, the velocity components by $r_1\Omega$, the time by $r_1\Omega/d$, and the pressure by $\rho r_1^2\Omega^2$ where ρ is the fluid density. The Reynolds number is $Re=\Omega r_1 d/\nu$, where ν is the kinematic viscosity.

The boundary conditions are $u=w=0$, $v=1$ when $r=r_i$ and $u=v=w=0$ when

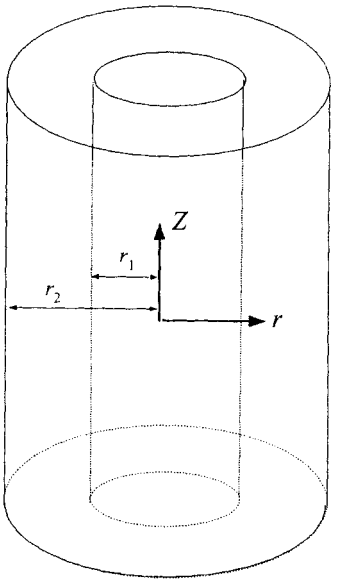

FIGURE 1. Geometry and coordinates.

$r = r_0$, where $r_i = r_1/d$ and $r_o = r_2/d$. Equations (1) admit a steady solution $u = w = 0$, $v = V(r) = A_o r + B_o/r$, where $A_o = -\eta/(1+\eta)$, $B_o = \eta/[(1+\eta)(1-\eta)^2]$ and $\eta = r_1/r_2$ is the radius ratio. The stability of this circular Couette flow is studied by superposing a disturbance and writing the disturbed velocity field as $(u, v, w) = (u', V(r)+v', w')$, where the primes denote disturbance quantities. Note that the magnitude of the disturbances does not have to be small in our formulation. Following Yao & Ghosh Moulic (1995*b*), the disturbance quantities are expressed in their most general form as integrals over all possible axial wavenumbers and Fourier series over the integer azimuthal wavenumbers. Thus, the azimuthal velocity is written as

$$v'(r,\phi,z,t) = \sum_{-\infty}^{\infty} \int_{-\infty}^{\infty} \hat{v}(k,n,r,t)\, e^{ikz+in\phi}\, dk. \tag{2}$$

The disturbance equations in Fourier space may be expressed as

$$\left.\begin{aligned} &D\hat{u}(k,n,r,t) + \frac{\hat{u}(k,n,r,t)}{r} + \frac{in\hat{v}(k,n,r,t)}{r} + ik\hat{w}(k,n,r,t) = 0, \\ &\frac{\partial \hat{u}_j}{\partial t}(k,n,r,t) + L_j(k,n,\hat{\boldsymbol{u}}(k,n,r,t), \hat{p}(k,n,r,t)) = \hat{N}_j(k,n,r,t), \end{aligned}\right\} \tag{3}$$

where $(\hat{u}_1, \hat{u}_2, \hat{u}_3) = (\hat{u}, \hat{v}, \hat{w})$, and L_j denote linear operators given by

$$L_1(k,n,\hat{\boldsymbol{u}},p) = -\frac{1}{Re}\left[L\hat{u} - \frac{\hat{u}}{r^2} - \frac{2in\hat{v}}{r^2}\right] + D\hat{p} - \frac{2V(r)\hat{v}}{r} + \frac{inV(r)\hat{u}}{r},$$

$$L_2(k,n,\hat{\boldsymbol{u}},\hat{p}) = -\frac{1}{Re}\left[L\hat{v} - \frac{\hat{v}}{r_2} + \frac{2in\hat{u}}{r^2}\right] + \frac{in\hat{p}}{r} + \left[DV + \frac{V}{r}\right]\hat{u} + \frac{inV(r)\hat{v}}{r},$$

$$L_3(k,n,\hat{\boldsymbol{u}},\hat{p}) = -\frac{1}{Re}L\hat{w} + ik\hat{p} + \frac{inV(r)\hat{w}}{r},$$

$$L \equiv D^2 + \frac{1}{r}D - \frac{n^2}{r^2} - k^2, \quad D \equiv \frac{d}{dr},$$

and $\hat{N}_j$ represent the nonlinear inertia terms in Fourier space defined by

$$\hat{N}_j(k,n,r,t) = -\frac{1}{(2\pi)^2}\int_{-\infty}^{\infty}\int_{0}^{2\pi}(\boldsymbol{u}'\cdot\nabla u_j')\,\mathrm{e}^{-\mathrm{i}kz-\mathrm{i}n\phi}\,\mathrm{d}\phi\,\mathrm{d}z. \tag{4a}$$

Equation (4a) may be expressed in convolution form as

$$\hat{N}_j(k,n,r,t) = -\sum_{n_1=-\infty}^{\infty}\int_{-\infty}^{\infty}\hat{\mathrm{M}}_j(k,n,\hat{\boldsymbol{u}}(k_1,n_1),\hat{\boldsymbol{u}}(k-k_1,n-n_1))\,\mathrm{d}k_1, \tag{4b}$$

where the operators M_j are given by

$$\mathrm{M}_1(k,n,\hat{\boldsymbol{u}}(k_1,n_1)\,\hat{\boldsymbol{u}}(k-k_1,n-n_1)) = \mathrm{D}^*[\hat{u}(k_1,n_1)\,\hat{u}(k-k_1,n-n_1)]$$
$$+\frac{\mathrm{i}n\hat{v}(k_1,n_1)\,\hat{u}(k-k_1,n-n_1)}{r}+\mathrm{i}k\hat{w}(k_1,n_1)\,\hat{u}(k-k_1,n-n_1)-\frac{\hat{v}(k_1,n_1)\,\hat{v}(k-k_1,n-n_1)}{r},$$

$$\mathrm{M}_2(k,n,\hat{\boldsymbol{u}}(k_1,n_1),\hat{\boldsymbol{u}}(k-k_1,n-n_1)) = \mathrm{D}^*[\hat{u}(k_1,n_1),\hat{v}(k-k_1,n-n_1)]$$
$$+\frac{\mathrm{i}n\hat{v}(k_1,n_1)\,\hat{v}(k-k_1,n-n_1)}{r}+\mathrm{i}k\hat{w}(k_1,n_1)\,\hat{v}(k-k_1,n-n_1)+\frac{\hat{u}(k_1,n_1)\,\hat{v}(k-k_1,n-n_1)}{r},$$

$$\mathrm{M}_3(k,n,\hat{\boldsymbol{u}}(k_1,n_1),\hat{\boldsymbol{u}}(k-k_1,n-n_1)) = \mathrm{D}^*[\hat{u}(k_1,n_1)\,\hat{w}(k-k_1,n-n_1)]$$
$$+\frac{\mathrm{i}n\hat{v}(k_1,n_1)\,\hat{w}(k-k_1,n-n_1)}{r}+\mathrm{i}k\hat{w}(k_1,n_1)\,\hat{w}(k-k_1,n-n_1),$$

and $\mathrm{D}^* \equiv \mathrm{D}+1/r$. Equations (3) have to be solved subject to the homogenous boundary conditions at $r = r_i$ and $r = r_o$.

The linear stability of the circular Couette flow may be studied by assuming the disturbance to be infinitesimally small, neglecting the nonlinear terms in equation (3), and expressing the Fourier components of the disturbance quantities in separable form as

$$\hat{u}(k,n,r,t) = \tilde{u}(k,n,r)\,\mathrm{e}^{-\mathrm{i}\omega(k,n)t},$$

where $\omega(k,n) = \omega^R(k,n)+\mathrm{i}\omega^I(k,n)$ is the complex frequency for the wavenumbers (k,n), and the superscripts R and I denote the real and imaginary parts of the complex frequency. The linearized disturbance equations may be written as

$$\left.\begin{aligned}&\mathrm{D}\tilde{u}(k,n,r)+\frac{\tilde{u}(k,n,r)}{r}+\frac{\mathrm{i}n\tilde{v}(k,n,r)}{r}+\mathrm{i}k\tilde{w}(k,n,r) = 0,\\ &\mathrm{L}_j(k,n,\tilde{u}(k,n,r),\tilde{p}(k,n,r)) = \mathrm{i}\omega(k,n)\,\tilde{u}(k,n,r).\end{aligned}\right\} \tag{5}$$

Equations (5) with the appropriate homogeneous boundary conditions form an eigenvalue problem for the complex frequency $\omega(k,n)$.

The solution of the nonlinear disturbance equations (3) may be expressed as

$$\hat{u}(k,n,r,t) = \sum_{m=1}^{\infty} A_m(k,n,t)\,\tilde{u}_m(k,n,r), \tag{6}$$

where $\tilde{u}_m(k,n,r)$ is the eigenfunction of the linearized equations (5) corresponding to the mth eigenvalue $\omega_m(k,n)$, and $A_m(k,n,t)$ is a time-dependent amplitude-density function. The eigenvalues of the linear stability operator are ordered so that $\omega_1^I \geqslant \omega_2^I \geqslant \omega_3^I \geqslant \ldots$. Thus, the first eigenvalue represents the least stable or the most unstable mode. The eigenfunctions are normalized so that

$$\int_{r_i}^{r_o}[|\tilde{u}_m|^2+|\tilde{v}_m|^2+|\tilde{w}_m|^2]\,r\,\mathrm{d}r = 1.$$

A governing equation for the amplitude density functions is determined by substituting the eigenfunction expansion (6) into the disturbance equations (3) and using the orthogonality relation between the eigenfunctions $\tilde{u}(k,n,r)$ of the linearized equations (5) and the corresponding adjoint eigenfunctions $\boldsymbol{u}^t(k,n,r) = (u^t(k,n,r), v^t(k,n,r), w^t(k,n,r))$. We define an inner product between the vectors $\tilde{\boldsymbol{u}}$ and $\boldsymbol{u}^t$ by

$$\langle \tilde{\boldsymbol{u}}, \boldsymbol{u}^t \rangle = \langle \tilde{u}, u^t \rangle + \langle \tilde{v}, v^t \rangle + \langle \tilde{w}, w^t \rangle,$$

where the inner product between two scalar functions $f(r)$ and $g(r)$ is defined as

$$\langle f, g \rangle = \int_{r_i}^{r_o} f^* g \, \mathrm{d}r,$$

and the asterisk denotes a complex conjugate. If the adjoint eigenfunctions are normalized so that

$$\langle u^t_m(k,n,r), \tilde{u}_j(k,n,r) \rangle = \delta_{j,m},$$

where $\delta_{j,m}$ is the Kronecker delta, use of the orthogonality property of the eigenfunctions and the continuity equation yields the following system of equations for the amplitude-density function:

$$\frac{\mathrm{d}A_m}{\mathrm{d}t} + \mathrm{i}\omega_m A_m = \langle u^t_m, \hat{N} \rangle, \tag{7a}$$

where $\hat{N} = (\hat{N}_1, \hat{N}_2, \hat{N}_3)$. Using (4*b*), equation (7*a*) may be expressed as

$$\frac{\mathrm{d}A_m}{\mathrm{d}t} + \mathrm{i}\omega_m A_m = \sum_{m_1=1}^{\infty} \sum_{m_2=1}^{\infty} \sum_{n_1=-\infty}^{\infty} I(k,n,m,m_1,m_2,n_1,t), \tag{7b}$$

where

$$I = \int_{-\infty}^{\infty} b(k_1, k-k_1, n_1, n-n_1, m_1, m_2, m) \, A_{m_1}(k_1, n_1) \, A_{m_2}(k-k_1, n-n_1) \, \mathrm{d}k_1,$$

and

$$b = \langle \boldsymbol{u}^t_m(k,n), \boldsymbol{M}(k,n, \tilde{\boldsymbol{u}}_{m_1}(k_1,n_1), \tilde{\boldsymbol{u}}_{m_2}(k-k_1, n-n_1)) \rangle,$$

where $\boldsymbol{M} = (M_1, M_2, M_3)$, depending on the eigenfunctions of the linearized equations (5). The details of the analysis can be found in Ghosh Moulic (1993).

The eigenfunction expansion used in the current formulation implicitly assumes that the linear-stability operator has an infinite set of discrete eigenvalues and a corresponding infinite set of eigenfunctions which form a complete set. While there is no general proof of the completeness of the linear-stability eigenfunctions, it is worth pointing out that DiPrima & Mabetler (1969) have proved a completeness theorem for a general class of non-self-adjoint eigenvalue problems in a finite domain. Using this theorem, they have demonstrated that the linear-stability operator for the Taylor problem has a complete set of eigenfunctions.

The eigenfunction expansion (6) has reduced the three momentum equations and the continuity equation to the system of integro-differential equations for the amplitude-density functions (7). Thus, a solution of (7) is a direct numerical solution of the Navier–Stokes equations. The linear terms on the left-hand side of (3), which include the convection and distortion of the disturbance waves by the mean flow and the diffusion of momentum, are reduced to a single term in (7) which describes the growth or decay of the wave in the generalized coordinates of the eigenfunctions. This simplification drastically reduces the CPU time required to complete the solution.

The system of integro-differential equations (7) is solved numerically. The infinite range of integration in the Fourier integrals representing the disturbance of a continuous spectrum is truncated to a finite range. The Fourier integrals are discretized

using the trapezoidal rule with uniform mesh size $\Delta k = 2k_{max}/N_z$, where k_{max} is the absolute maximum wavenumber and N_z is the number of waves in the axial direction. The infinite Fourier series in the azimuthal direction is also truncated to a finite series involving N_ϕ terms. The eigenfunctions are obtained by solving the linear-stability equations by a Chebyshev collocation method using N_r points, that is using $N_r - 1$ Chebyshev polynomials. A complex QZ algorithm (Moler & Stewart 1973) is used to determine the eigenvalues and eigenvectors. We sort the linear stability eigenmodes in increasing order of the imaginary part of the complex frequency, $\omega_m^I(k, n)$. A time-splitting scheme is used for the temporal discretization. The nonlinear terms are approximated by an explicit second-order-accurate Adams–Bashforth scheme, while the linear term is approximated by an implicit second-order-accurate Crank–Nicholson scheme. The time-splitting scheme has the dual advantage of avoiding iterations for the nonlinearities and avoiding a stringent Courant-number restriction for numerical stability due to linear terms. The convolution integrals are evaluated by a pseudospectral method using a fast Fourier transformation and aliasing errors are removed by padding using the two-thirds rule (Canuto *et al.* 1988). Several different grid sizes have been tested to ensure the convergence of the numerical computations. The results have also been checked with a direct numerical simulation of the time-dependent Navier–Stokes equations using the spectral method of Fourier–Chebyshev expansions starting with the same initial conditions. Complete agreement is found between these two numerical solutions. This is expected since both computations represent exact numerical solutions of the Navier–Stokes equations. The computations were performed on the CRAY C-90 supercomputer at the Pittsburgh Supercomputer Center.

3. Results and discussion

Results have been obtained for two different radius ratios $\eta = 0.5$ and $\eta = 0.874$. The radius ratio 0.5 corresponds to the apparatus used in the experiments of Snyder (1969), while 0.874 corresponds to the apparatus used by Coles (1965). Results are presented in figures 2 and 3 for $\eta = 0.5$ and $Re = 88.1$. Results obtained for $\eta = 0.874$ and $Re = 162$ are presented in figures 4–7. Linear-stability analysis indicates that for $\eta = 0.5$ and $Re = 88.1$, circular Couette flow is unstable to rotationally symmetric disturbances with axial wavenumbers lying between 1.6 and 5.6. At $Re = 162$ and $\eta = 0.874$, circular Couette flow is linearly unstable to disturbances with azimuthal wavenumbers 0, 1, 2, 3, 4, 5 and 6. The range of axial wavenumbers for linearly unstable disturbances lies between 1.5 and 5.75 for $n = 0$ and 1, between 1.75 and 5.75 for $n = 2$, between 2 and 5.5 for $n = 3$, between 2.25 and 5.25 for $n = 4$, between 2.75 and 4.75 for $n = 5$, and between 3.5 and 3.75 for $n = 6$. The system of integro-differential equation (7*a*) was solved numerically with different initial conditions using 20 eigenmodes for each wavenumber, that is using 20 terms in eigenfunction expansion given by equation (6). The integrals in (7*a*) were discretized by the trapezoidal rule using a uniform mesh size $\Delta k = 0.25$ for $\eta = 0.5$, $Re = 88.1$ and $\Delta k = 0.5$ for $\eta = 0.874$, $Re = 162$. The infinite range of integration was truncated to $-12 \leqslant k \leqslant 12$, which was found to be adequate as the kinetic energies of the high-wavenumber modes were negligible. The infinite sum over the azimuthal wavenumbers was truncated to $-20 \leqslant n \leqslant 20$ for $\eta = 0.874$ and $Re = 162$. At $Re = 88.1$ and $\eta = 0.5$, circular Couette flow is linearly stable to non-rotationally symmetric disturbances, and the computations for this case were done assuming the disturbance to be rotationally symmetric in order to save computer time.

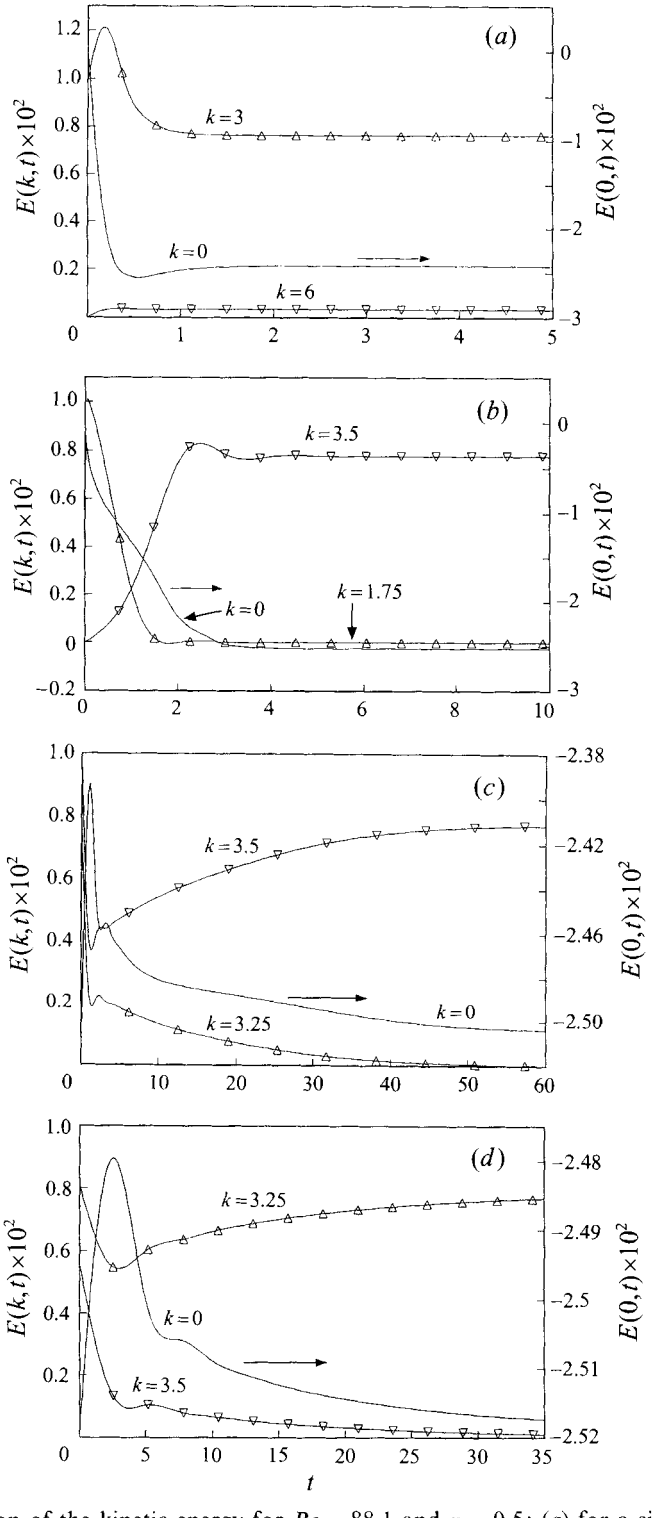

FIGURE 2. Evolution of the kinetic energy for $Re = 88.1$ and $\eta = 0.5$: (*a*) for a single initial mode $k = 3$; (*b*) for a single initial mode $k = 1.75$; (*c*) for two initial modes at $k = 3.25$ and 3.5 where the initial amplitude at $k = 3.5$ is larger; (*d*) as (*c*) but the initial amplitude at $k = 3.25$ is larger.

3.1. *Taylor-vortex flows*

Figure 2(*a*) shows the results of a numerical solution of the integro-differential equations (7*a*) for $\eta = 0.5$ and $Re = 88.1$ in which the initial disturbance consists of a single dominant mode with wavenumber $k = 3$. The evolution of the kinetic energies of the dominant wave components is plotted in figure 2(*a*). For rotationally symmetric flows, the kinetic energy of the Fourier component with axial wavenumber k is given by

$$E(k,t) = \begin{cases} \displaystyle\int_{r_i}^{r_o} r[|\hat{u}|^2 + |\hat{v}|^2 + |\hat{w}|^2]\,\mathrm{d}r, & k \neq 0 \\ \displaystyle\frac{1}{2}\int_{r_i}^{r_o} r[|V+\hat{v}|^2 - V^2]\,\mathrm{d}r, & k = 0. \end{cases} \tag{8}$$

Equation (8) accounts for the energy in both modes $\pm k$. The kinetic energy of the circular Couette flow is substracted from the mean-flow kinetic energy in (8) so that $E(0,t)$ represents the kinetic energy associated with the distortion of the mean flow. The mode $k = 3$ is linearly unstable, and grows initially at the rate predicted by linear stability theory. Nonlinear interactions generate harmonics of the wave $k = 3$ and induce a mean-flow distortion ($k = 0$). As the amplitude of the mode $k = 3$ increases, nonlinear effects become important and alter the growth rate, causing the mode to decay and eventually reach an equilibrium state. The energy is taken from the mean flow to support the disturbance wave and its harmonics. Table 1 shows the amplitudes $\bar{A}_m(k) = \Delta k\,|A_m(k, n=0)|$ of the first ten eigenmodes of the different harmonic components of the disturbance in this equilibrium state, where $|A_m(k,n)|$ denotes the magnitude of the complex amplitude density function. Table 2 gives the corresponding frequencies $\mathrm{d}\beta_m(k)/\mathrm{d}t$ of the various eigenmodes, where $\beta_m = \tan^{-1}(A_m^I/A_m^R)$ is the phase angle of the complex amplitude-density function $A_m(k,n)$. A glance at table 2 reveals that most of the eigenmodes have zero frequencies, that is they represent a stationary disturbance. However, some of the eigenmodes have non-zero frequencies. These eigenmodes represent a time-periodic disturbance. A close examination of table 2 shows that the time-periodic eigenmodes for a given wavenumber occur in pairs which have frequencies of the same magnitude but opposite sign. For instance, the fourth and fifth eigenmodes of the wavenumber $k = 3$ have frequencies of 0.0105 and -0.0105 respectively. These two eigenmodes represent travelling waves which move in opposite directions with the same wave speed. Other such pairs are formed by the fourth–seventh eigenmodes of the wavenumber $k = 6$, the sixth and seventh eigenmodes of the wavenumbers $k = 9$, and the sixth–ninth eigenmodes of the wavenumber $k = 12$. These eigenmodes in bold in table 2 can carry disturbances from the ends of an annulus into its interior. Table 1 indicates that the eigenmodes of each of these pairs have the same amplitude. For instance, the fourth and fifth eigenmodes of the wavenumber $k = 3$ have the same amplitude 0.004497, the fourth and fifth eigenmodes of the wavenumber $k = 6$ have the same amplitude 0.00512, etc. The superposition of all the eigenmodes results in a standing wave pattern. Any disturbance which destroys the symmetry of the standing waves can result in the addition of components of spiral flows. Table 1 shows that the amplitudes of the time-periodic eigenmodes is an order of magnitude smaller than the amplitude of the stationary Taylor-vortex cell. This may explain why spiral flows have not been identified in experiments on rotationally symmetric Taylor-vortex flows.

Figure 2(*b*) shows the results of a numerical solution of the integro-differential equation (7*a*) at $Re = 88.1$ and $\eta = 0.5$ starting with a single dominant mode with

m	$k=0$	$k=3$	$k=6$	$k=9$	$k=12$
1	0.3641×10^{-1}	0.8650×10^{-1}	0.1772×10^{-1}	0.3229×10^{-2}	0.8255×10^{-3}
2	0.1957×10^{-11}	0.8714×10^{-2}	0.1145×10^{-2}	0.1072×10^{-3}	0.1986×10^{-3}
3	0.4582×10^{-1}	0.4474×10^{-2}	0.5770×10^{-2}	0.8343×10^{-3}	0.3437×10^{-4}
4	0.3007×10^{-11}	$\mathbf{0.4497\times10^{-2}}$	$\mathbf{0.5120\times10^{-2}}$	0.5860×10^{-3}	0.5571×10^{-4}
5	0.1273×10^{-2}	$\mathbf{0.4497\times10^{-2}}$	$\mathbf{0.5120\times10^{-2}}$	0.4384×10^{-3}	0.9338×10^{-4}
6	0.1076×10^{-11}	0.5323×10^{-3}	$\mathbf{0.1131\times10^{-2}}$	$\mathbf{0.2789\times10^{-3}}$	$\mathbf{0.7535\times10^{-4}}$
7	0.1416×10^{-2}	0.5030×10^{-4}	$\mathbf{0.1131\times10^{-2}}$	$\mathbf{0.2789\times10^{-3}}$	$\mathbf{0.7535\times10^{-4}}$
8	0.9047×10^{-12}	0.2625×10^{-3}	0.5979×10^{-3}	0.3127×10^{-3}	$\mathbf{0.6523\times10^{-4}}$
9	0.8591×10^{-4}	0.2808×10^{-3}	0.1584×10^{-3}	0.1638×10^{-3}	$\mathbf{0.6523\times10^{-4}}$
10	0.6120×10^{-13}	0.2142×10^{-4}	0.5842×10^{-4}	0.4279×10^{-4}	0.1827×10^{-4}

TABLE 1. Amplitudes of the different eigenmodes for $Re = 88.1$ and $\eta = 0.5$ for a single initial mode with $k = 3$

m	$k=0$	$k=3$	$k=6$	$k=9$	$k=12$
1	2.45×10^{-16}	3.44×10^{-12}	6.89×10^{-12}	1.03×10^{-11}	1.38×10^{-11}
2	2.45×10^{-16}	3.44×10^{-12}	6.89×10^{-12}	1.03×10^{-11}	1.38×10^{-11}
3	2.45×10^{-16}	3.44×10^{-12}	6.89×10^{-12}	1.03×10^{-11}	1.38×10^{-11}
4	2.45×10^{-16}	**0.0105**	**−0.0097**	1.03×10^{-11}	1.38×10^{-11}
5	2.45×10^{-16}	**−0.0105**	**0.0097**	1.03×10^{-11}	1.38×10^{-11}
6	2.45×10^{-16}	3.44×10^{-12}	**−0.0123**	**−0.0214**	**0.0235**
7	2.45×10^{-16}	3.45×10^{-12}	**0.0123**	**0.0214**	**−0.0235**
8	2.45×10^{-16}	3.44×10^{-12}	6.89×10^{-12}	1.03×10^{-11}	**0.0151**
9	2.45×10^{-16}	3.44×10^{-12}	6.89×10^{-12}	1.03×10^{-11}	**−0.0151**
10	2.45×10^{-16}	3.44×10^{-12}	6.89×10^{-12}	1.03×10^{-11}	1.38×10^{-11}

TABLE 2. Frequencies of the different eigenmodes for $Re = 88.1$ and $\eta = 0.5$ for a single initial mode with $k = 3$

wavenumber $k = 1.75$. The mode $k = 1.75$ is linearly unstable. However, unlike the previous case, the mode $k = 1.75$ decays to zero instead of growing to a finite-amplitude equilibrium state, while its harmonic $k = 3.5$, excited through nonlinear wave interaction, grows and reaches a supercritical equilibrium state. This result is in agreement with the Eckhaus and Benjamin–Feir side-band instability (Stuart & DiPrima 1978). The equilibrium state in this case also is a standing-wave pattern with a dominant stationary Taylor-vortex cell and some oscillatory modes of much smaller amplitudes. However, the dominant wave in this case has a wavenumber $k = 3.5$ in contrast to the previous case which had a dominant wavenumber $k = 3$.

The results of figures 2(*a*) and 2(*b*) indicate that the equilibrium state of the flow is not uniquely determined by the Reynolds number and radius ratio of the cylinders, but depends on the waveform of the initial disturbance. Multiple stable equilibrium states can occur at the same Reynolds number. We have computed several stable rotationally symmetric Taylor-vortex flows for $\eta = 0.5$ and $Re = 88.1$ by integrating (7*a*) starting with initial conditions consisting of a single linearly unstable mode of small initial amplitude. In all of these cases, the final equilibrium state was a monochromatic standing wave with a single dominant wavenumber and its harmonies. The standing wave pattern consists of a dominant stationary Taylor-vortex cell and some low-frequency oscillatory modes of much smaller amplitudes. Our computations indicate that the range of wavenumbers for stable supercritical Taylor vortices is narrower than the span of the neutral curve of linear stability theory, in agreement with the Eckhaus

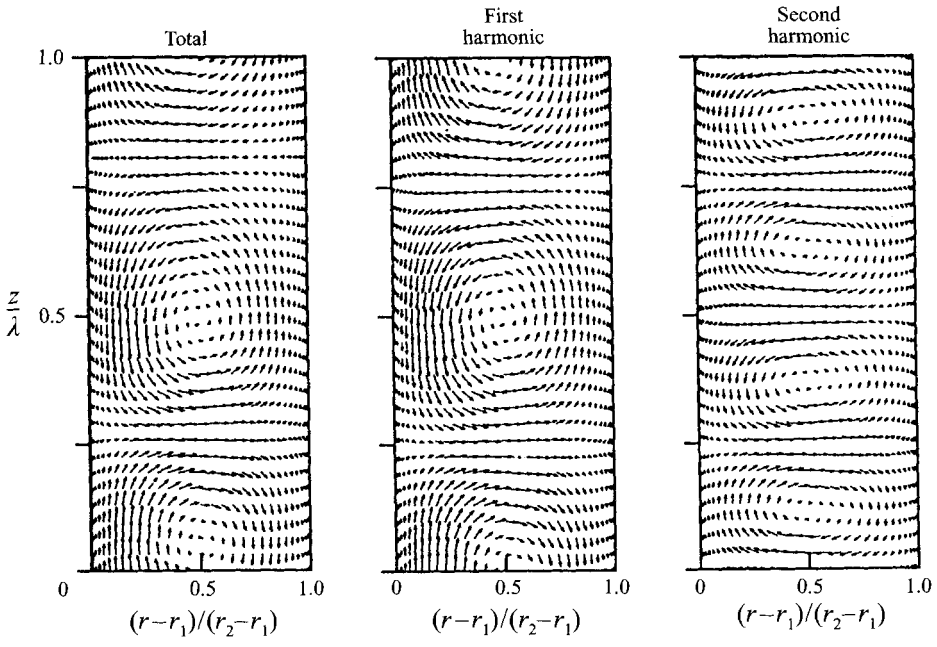

FIGURE 3. Projection of the velocity vectors for Taylor-vortex flow onto the (r, z)-plane for $Re = 88.1$, $\eta = 0.5$ and $k = 3.5$.

and Benjamin–Feir sideband instability mechanisms (Stuart & DiPrima 1978). When the initial disturbance consists of a single dominant mode with wavenumber inside this narrow band, the initial wave remained the dominant wave in the equilibrium state, as in the case illustrated by figure 2(*a*). When the initial disturbance consists of a single dominant mode with wavenumber outside this narrow band but within the unstable region of linear theory, the initial wave decayed, the energy being transferred to a wave inside the narrow band, which is excited through nonlinear wave interaction, as in figure 2(*b*). This indicates that a side-band instability is a consequence of nonlinear wave resonance.

We have examined the stability of some of these equilibrium states to finite-amplitude disturbances. Figures 2(*c*) and 2(*d*) show the results obtained by perturbing a stable supercritical Taylor-vortex flow in which the critical wavenumber $k = 3.25$ was the dominant wave with a disturbance which consists of a linearly unstable eigenmode with wavenumber $k = 3.5$. Figure 2(*c*) presents the results of a computation in which the initial perturbation was given an amplitude of 0.1, and indicates that the wave $k = 3.25$ decays to zero, while the wave $k = 3.5$ becomes the dominant wave in the equilibrium state. Figure 2(*d*) presents the results of a similar computation in which the initial perturbation was given an amplitude of 0.075. In this case, the perturbation decays to zero, and the critical wave remains dominant in the equilibrium state. Figures 2(*c*) and 2(*d*) indicate that the dominant wavenumber in the equilibrium state can be shifted by a disturbance of sufficiently large amplitude. This phenomenon can have practical significance in engineering applications.

Figure 3 shows the projection of the velocity vectors for the equilibrium state depicted by figure 2(*b*) onto the (r, z)-plane. The first and second harmonic components of the velocity vectors are also shown in figure 3, along with the total velocity vectors. The figure indicates that the velocity vectors of the second harmonic near the inflow boundary of the Taylor vortex are opposite in direction to the velocity vectors of the

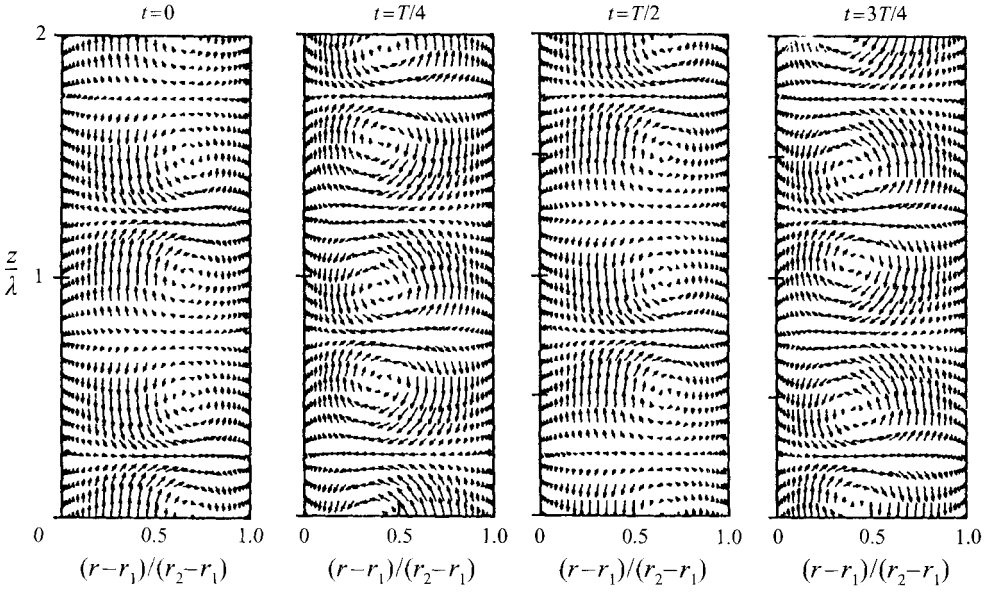

FIGURE 4. Projection of the velocity vectors for wavy-vortex flow onto (r, z)-plane for $Re = 162$, $\eta = 0.874$, $k = 3$, $n = 4$ at equilibrium.

first harmonic. The velocity vectors of the second harmonic near the outflow boundary of the Taylor vortex, on the other hand, are in the same direction as those of the first harmonic. Thus, the second harmonic component of the disturbance, generated through nonlinear wave interaction, tends to reduce the radial velocity of the inflow boundary jet between the Taylor vortices and increase the radial velocity of the outflow boundary jet. Thus, the outflow boundary has a larger radial velocity than the inflow boundary. This agrees with previous numerical results (Marcus 1984).

It is worth noting that the results obtained using 15 and 20 eigenfunctions completely agree within the accuracy of our computation. A convergent result by a Fourier–Chebyshev spectral method, comparable to the expansion of 15 or 20 eigenfunctions, requires a minimum of 33 Chebyshev polynomials. The results presented in figures 2 and 3 are obtained using 20 eigenfunctions in the expansion (6). The required number of eigenfunctions in (6) for different Reynolds number can be determined by demanding that the amplitudes of the highest few eigenmodes are sufficiently close to zero. This means that (6) must be convergent in order to provide physically meaningful results.

We also found that, if the expansion (6) is severely truncated to, say, five or fewer eigenfunctions, the results are qualitatively different from the convergent results for the same initial conditions; sometimes, the results may become numerically unstable and diverge. This is due to the lack of a dissipative mechanism in a severely truncated system. The higher eigenmodes corresponding to larger ω_m^I are more dissipative in nature, and a sufficient number of eigenmodes is needed for numerical stability. Physically, this implies that a substantial dissipation occurs non-isotropically within the range of wavenumbers for energy-containing eddies. *Geometrically, one visualizes that a substantial dissipation occurs in thin layers whose sizes along the axial and the azimuthal directions are comparable to the energy-containing eddies.* The equilibrium waves of larger wavenumbers are the harmonics of the dominant wave, are dynamically inert and are not particularly more dissipative. Their small amplitudes are the consequence of little energy being transferred to them nonlinearly. Similar conclusions can be made for the subharmonics of the dominant wave.

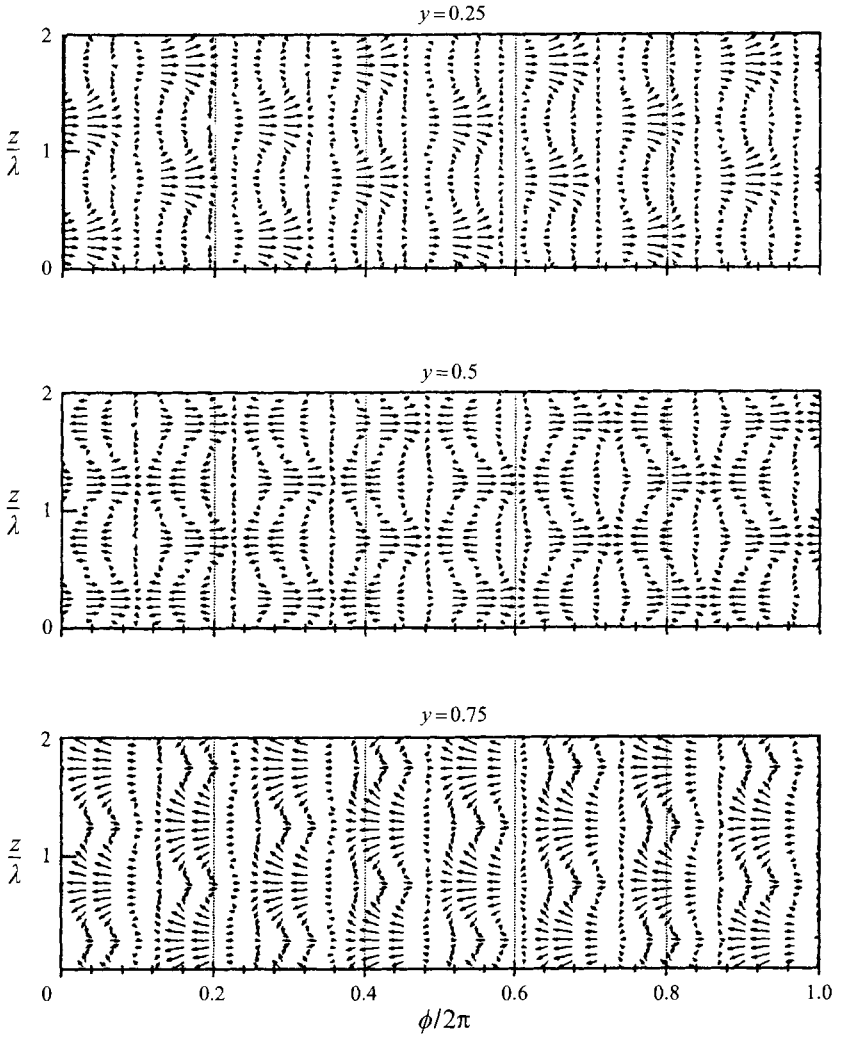

FIGURE 5. Projection of the velocity vectors for wavy-vortex flow onto (ϕ, z)-plane for $Re = 162$, $\eta = 0.874$, $k = 3$ and $n = 4$ at equilibrium.

3.2. *Wavy-vortex flows*

We have also computed several stable non-rotationally symmetric wavy-vortex flows for $\eta = 0.874$ and $Re = 162$. These equilibrium states consist of monochromatic travelling waves which propagate in the azimuthal direction. Thus, at a fixed location in space, these flows are periodic in time. A typical stable wavy-vortex equilibrium state with dominant axial wavenumber $k = 3$ and azimuthal wavenumber $n = 4$ is illustrated in figures 4 and 5. Figure 4 shows the projection of the velocity vectors onto the (r, z)-plane at a given azimuthal location at four different times $t = 0$, $T/4$, $T/2$ and $3T/4$ where T is the time period. The vertical line on the left-hand side represents the boundary of the inner cylinder, while the vertical line on the right-hand side represents the boundary of the outer cylinder. The flow is periodic in both the axial and azimuthal directions. In figure 4, two pairs of counter-rotating vortices, spread over two axial wavelengths $\lambda = 2\pi/k$, have been plotted. The figure indicates that the position of the vortices oscillates with time. Thus, the counter-clockwise-rotating vortex in the

	n	1	2	3	4
Wavy vortex	G_{wv}/G_C	1.44	1.36	1.28	1.20
Spiral	G_{sv}/G_C	1.51	—	—	1.32

TABLE 3. Variation of torque for $Re = 162$ and $\eta = 0.874$ with azimuthal wavenumber for $k = 3$

bottom half of the figure at time $t = 0$ moves upwards in the axial direction to a higher position at time $t = T/4$, its previous position being taken up by a clockwise-rotating vortex which has also been displaced upwards in the axial direction by the wave motion. The counter-clockwise-rotating vortex continues to move upwards to a slightly higher axial position at time $t = T/2$, and then moves downwards to a lower axial position at time $t = 3T/4$. At time $t = T$, the vortex reaches its original position at time $t = 0$, completing the cycle. As a consequence of the oscillation of the vortices, the surfaces separating the counter-rotating vortices are wavy.

The projection of the velocity vectors for this equilibrium state onto the (ϕ, z)-plane is shown in figure 5 at three radial locations $y = 0.25$, 0.5 and 0.75, where $y = (r-r_i)/(r_o-r_i)$ is a normalized radial coordinate, at a particular instant of time. The figure demonstrates that the flow is invariant under the transformation $\phi \rightarrow \phi + 2\pi/n$, where $n = 4$ is the azimuthal wavenumber in the equilibrium state. Thus, the flow pattern is repeated as the azimuthal angle is increased by $\pi/2$. The figure also demonstrates that there is no net flow in the axial direction. The wave front does not propagate in the axial direction. A close examination of figure 5 reveals that the sense of rotation of the vortices in the radial plane $y = 0.75$ is opposite to the sense of rotation of the corresponding vortices in the radial plane $y = 0.25$. This agrees with the sense of rotation of the vortices indicated in the projection of the velocity vectors onto the (r, z)-plane (figure 4).

The numerical results show that the azimuthal modes $n = 1$, 2, 3 and 4 are stable equilibrium states, but $n = 0$, 5 and 6 are unstable. An initial condition with azimuthal mode 0, 5 or 6 will decay and shift to a stable azimuthal mode. Owing to the limited computational resources, we did not continue our computation in order to find out what final stable equilibrium azimuthal mode would result from these unstable initial azimuthal modes. We did not find two travelling azimuthal waves in our computation because the selected Reynolds number is too low for the existence of a modulated wavy-vortex flow.

We have computed the torque on the inner cylinder for several wavy-vortex flows at $Re = 162$ and $\eta = 0.874$. The ratio of the wavy-vortex torque G_{wv} and that for circular Couette flow G_C is given in table 3 for wavy-vortex flows with dominant axial wavenumber $k = 3$ and azimuthal wavenumbers $n = 1$, 2, 3 and 4. The table indicates that the torque on the inner cylinder decreases monotonically as the aximuthal wavenumber increases. The increase in torque of the wavy-vortex flow relative to the corresponding torque of the unstable circular Couette flow varies from 44% for the wavy-vortex flow with aximuthal wavenumber $n = 1$ to 20% for azimuthal wavenumber $n = 4$ and the same axial wavenumber. This agrees with the trend predicted by Eagles (1974). Table 3 demonstrates that the torque induced by the fluid motion cannot be determined uniquely owing to the existence of multiple equilibrium states. Since the equilibrium state is not unique and depends on the initial conditions which cannot usually be controlled in real engineering systems, an uncertainty associated with non-uniqueness should be considered when using any accurately measured value of the torque in practice. We have not done an extensive study of the

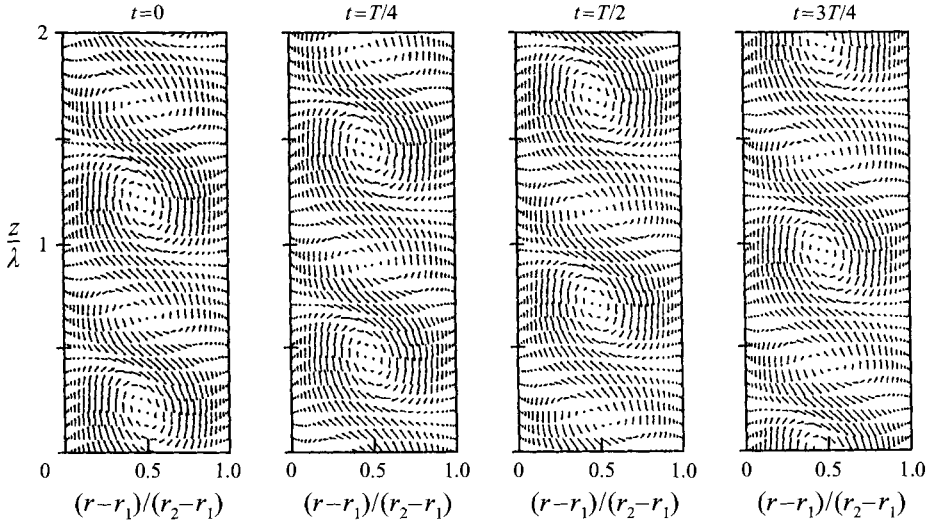

FIGURE 6. Projection of the velocity vectors for spiral-vortex flow onto the (r, z)-plane for $Re = 162$, $\eta = 0.874$, $k = 3$, $n = 4$ at equilibrium.

variation of the torque among all possible equilibrium states with different axial and azimuthal wavenumbers at $Re = 162$ and $\eta = 0.874$ as the required computer time is prohibitively high. It is reasonable to expect a larger uncertainty than that indicated in table 3 if one considers the effect of variation in the axial wavenumber as well as the azimuthal wavenumber. At higher Reynolds numbers, the range of linearly unstable wavenumbers will be larger. Consequently, the uncertainty in the torque will be higher.

3.3. *Spiral-vortex flows*

Spiral-vortex flows have been found when the outer cylinder is also rotating (Andereck, Liu & Swinney 1986). They found that two spirals exist separated by an interface located near the mid-plane. The interface varies with time and is not necessarily sharp. Sometimes the interface can be two to three times the size of the vortices and consists of the overlap of both the originally separate spirals. For the particular case, shown in their figure 4, the lower spiral eventually left the flow completely, leaving the upper spiral over the entire annulus. Their observation seems to suggest that spiral vortices resulted from the end condition of the rotating cylinders.

Our model assumes infinite-long cylinders with a stationary outer cylinder and cannot model the end conditions. Since the linear-instability eigenfunctions consist a pair of travelling waves which form standing waves along the axial direction at $Re = 162$ and $\eta = 0.874$, we select one travelling wave as the initial condition to destroy the symmetry of possible standing waves. This results in spiral vortices as shown in figure 6 for $k = 3$ and $n = 4$. The wave travels one wavelength over a period along the axial direction. This results in a net upward mass flow. If we select a downward travelling wave as the initial condition, then a downwardly travelling spiral-vortex flow will be the stable equilibrium state. The projection of the velocity vectors for this equilibrium state onto the (ϕ, z)-plane is shown in figure 7 at three radial locations $y = 0.25$, 0.5 and 0.75. It shares many similarities with those for a wavy-vortex flow. Two calculated torques G_{sv} for $n = 1$ and 4 are higher than those for wavy-vortex flows and are included in table 3.

The spiral-vortex flow for such a low Reynolds number, 162, has not been confirmed

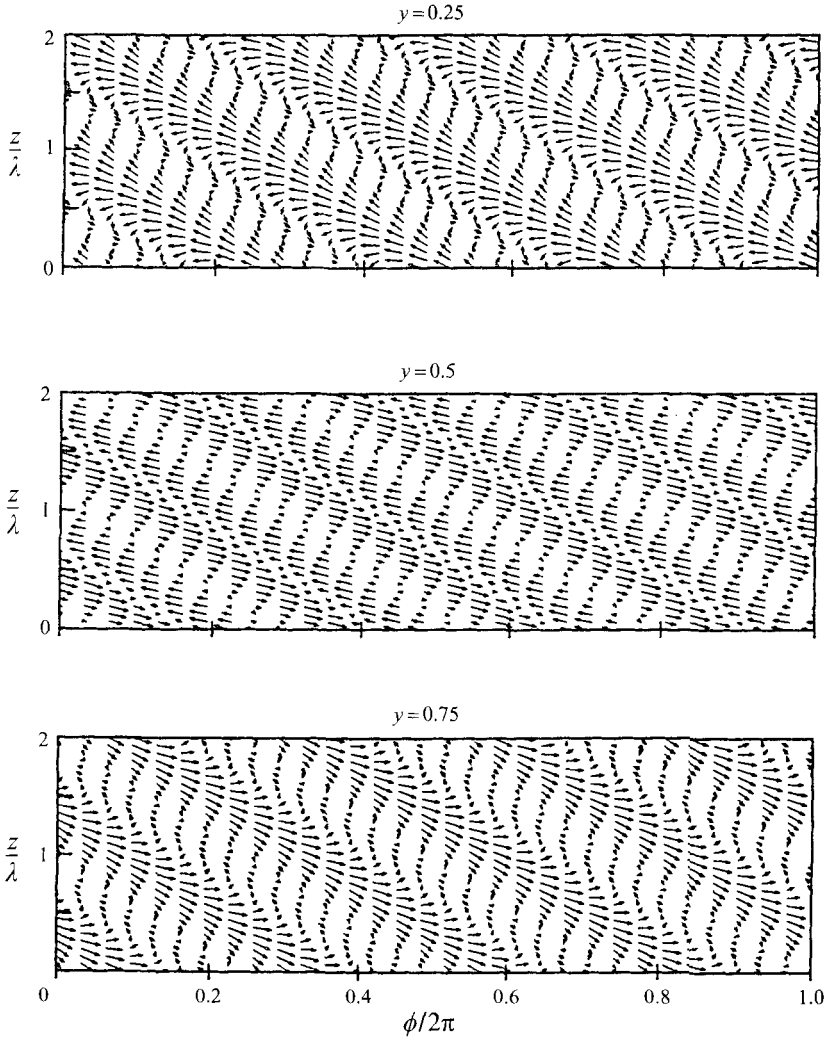

FIGURE 7. Projection of the velocity vectors for spiral-vortex flow onto the (ϕ, z)-plane for $Re = 162$, $\eta = 0.874$, $k = 3$ and $n = 4$ at equilibrium.

experimentally. Nevertheless, the numerical results seem to suggest that a richer flow structure may be possible than has so far been identified, if we known how to excite it.

4. Conclusion

The present study confirms that the supercritical equilibrium state of Taylor-vortex, wavy-vortex and spiral-vortex flows is not unique, but depends on the wave form of the initial disturbance, as observed experimentally. For all the equilibrium states in our study, the magnitude of the mean-flow distortion was larger than the amplitude of the waves. This is because energy, supplied by the external torque acting on the inner cylinder, is taken from the mean flow to support the disturbance wave and its harmonics. The solution of the integro-differential system (7) demonstrates that a rotationally symmetric Taylor-vortex flow is not a pure stationary wave, but is

composed of a dominant stationary vortex and some low-frequency oscillatory modes of small amplitudes whose superposition leads to a standing wave pattern. These oscillatory modes have not been identified in experiments on rotationally symmetric Taylor-vortex flow, possibly because of the small amplitude and low frequency of these wave components.

REFERENCES

ANDERECK, C. D., LIU, S. S. & SWINNEY, H. L. 1986 Flow regimes in a circular Couette system with independently rotating cylinders. *J. Fluid Mech.* **164**, 155–183.

BENJAMIN, T. B. 1978 Bifurcation phenomena in steady flows of a viscous fluid. II. Experiments. *Proc. R. Soc. Lond.* A **359**, 27–43.

BURKHALTER, J. E. & KOSCHMIEDER, E. L. 1974 Steady supercritical Taylor vortices after sudden starts. *Phys. Fluids* **17**, 1929–1935.

CANUTO, C., MUSSAINI, M. Y., QUARTERONI, A. & ZANG, T. A. 1988 *Spectral Methods in Fluid Dynamics*. Springer.

COLES, D. 1965 Transition in circular Couette flow. *J. Fluid Mech.* **21**, 385–425.

DAVEY, A., DIPRIMA, R. C. & STUART, J. T. 1968 On the instability of Taylor vortices. *J. Fluid Mech.* **31**, 17–52.

DIPRIMA, R. C. 1961 Stability of nonrotationally symmetric disturbances for viscous flow between rotating cylinders. *Phys. Fluids* **4**, 751–755.

DIPRIMA, R. C. & MABETLER, G. J. 1969 A completeness theorem for non-self-adjoint eigenvalue problems in hydrodynamic instability. *Arch. Rat. Mech. Anal.* **34**, 218–227.

EAGLES, P. M. 1974 On the torque of wavy vortices. *J. Fluid Mech.* **62**, 1–9.

FENSTERMACHER, P. R., SWINNEY, H. L. & GOLLUB, J. P. 1979 Dynamical instabilities and the transition to chaotic Taylor-vortex flow. *J. Fluid Mech.* **94**, 103–129.

GHOSH MOULIC, S. 1993 Nonlinear instability. PhD thesis, Department of Mechanical and Aerospace Engineering, Arizona State University.

KLEISER, L. & SCHUMANN, U. 1980 Treatment of incompressibility and boundary conditions in three-dimensional numerical spectral simulations of plane channel flows. *Proc. 3rd GAMM Conf. on Numerical Methods in Fluid Mechanics* (ed. E. H. Hirschel), pp. 165–173. Vieweg.

KRUEGER, E. R., GROSS, A. & DIPRIMA, R. C. 1966 On the relative importance of Taylor-vortex and non-axisymmetric modes in flow between rotating cylinders. *J. Fluid Mech.* **24**, 521–538.

MARCUS, P. S. 1984 Simulation of Taylor–Couette flow. Part 2. Numerical results for wavy-vortex flow with one traveling wave. *J. Fluid Mech.* **146**, 65–113.

MOLER, C. B. & STEWART, G. W. 1973 An algorithm for generalized matrix eigenvalue problems. *SIAM J. Numer. Anal.* **10**, 241–256.

SNYDER, H. A. 1969 Wavenumber selection at finite amplitude in rotating Couette flow. *J. Fluid Mech.* **35**, 273–298.

STUART, J. T. & DIPRIMA, R. C. 1978 The Eckhaus and Benjamin–Feir resonstance mechanisms. *Proc. R. Soc. Lond.* A **362**, 27–41.

TAYLOR, G. I. 1923 Stability of a viscous liquid contained between two rotating cylinders. *Phil. Trans R. Soc. Lond.* A **223**, 289–343.

YAO, L. S. 1995 Non-uniqueness in convection. In *Symp. on Thermal Science and Engineering in Honor of Chancellor Chang-Lin Ten, Berkeley, California, November 14* (ed. R. O. Buckins), pp. 75–82. University of Illinois at Urbana-Champaign.

YAO, L. S. & GHOSH MOULIC, S. 1994 Uncertainty of convection. *Intl J. Heat Mass Transfer* **37**, 1713–1721.

YAO, L. S. & GHOSH MOULIC, S. 1995*a* Taylor–Couette instability with a continuous spectrum. *Trans. ASME* E: *J. Appl. Mech.* **62**, 915–923.

YAO, L. S. & GHOSH MOULIC, S. 1995*b* Nonlinear instability of traveling waves with a continuous spectrum. *Intl J. Heat Mass Transfer* **38**, 1751–1772.